processes

MDPI

Article

Activated Carbon Aerogel as an Electrode with High Specific Capacitance for Capacitive Deionization

Wei Wang [1,2], Kerui Li [1,3], Ge Song [1], Minghua Zhou [1,*] and Peng Tan [1]

[1] MOE Key Laboratory of Pollution Processes and Environmental Criteria, Tianjin Key Laboratory of Environmental Technology for Complex Trans-Media Pollution, Tianjin Advanced Water Treatment Technology International Joint Research Center, College of Environmental Science and Engineering, Nankai University, Tianjin 300350, China
[2] Nankai Cangzhou Bohai New Area Green Chemical Research Co., Ltd., Cangzhou 061108, China
[3] China Railway Academy Co., Ltd., Chengdu 610032, China
* Correspondence: zhoumh@nankai.edu.cn; Tel.: +86-022-23501117

Abstract: In this study, carbon aerogels (CAs) were synthesized by the sol-gel method, using environmentally friendly glucose as a precursor, and then they were further activated with potassium hydroxide (KOH) to obtain activated carbon aerogels (ACAs). After the activation, the electrochemical performance of the ACAs was significantly improved, and the specific capacitance increased from 19.70 $F{\cdot}g^{-1}$ to 111.89 $F{\cdot}g^{-1}$. Moreover, the ACAs showed a stronger hydrophilicity with the contact angle of 118.54° compared with CAs (69.31°). When used as an electrode for capacitive deionization (CDI), the ACAs had not only a better diffuse electric double layer behavior, but also a lower charge transfer resistance and intrinsic resistance. Thus, the ACA electrode had a faster CDI desalination rate and a higher desalination capacity. The unit adsorption capacity is three times larger than that of the CA electrode. In the desalination experiment of 100 $mg{\cdot}L^{-1}$ sodium chloride (NaCl) solution using a CDI device based on the ACA electrode, the optimal electrode spacing was 2 mm, the voltage was 1.4 V, and the flow rate was 30 $mL{\cdot}min^{-1}$. When the NaCl concentration was 500 $mg{\cdot}L^{-1}$, the unit adsorption capacity of the ACA electrode reached 26.12 $mg{\cdot}g^{-1}$, much higher than that which has been reported in many literatures. The desalination process followed the Langmuir model, and the electro-sorption of the NaCl was a single layer adsorption process. In addition, the ACA electrode exhibited a good regeneration performance and cycle stability.

Keywords: carbon aerogel; activation; capacitive deionization; desalination; electro-sorption

Citation: Wang, W.; Li, K.; Song, G.; Zhou, M.; Tan, P. Activated Carbon Aerogel as an Electrode with High Specific Capacitance for Capacitive Deionization. *Processes* **2022**, *10*, 2330. https://doi.org/10.3390/pr10112330

Academic Editor: Suresh K. Bhatia

Received: 11 October 2022
Accepted: 4 November 2022
Published: 9 November 2022

1. Introduction

The rapid population growth and industrial development have led to a global shortage of water resources. At the same time, the discharge of pollutants in the environment has caused a decline in water quality, even in water-rich areas. To solve the water crisis, extensive researches have been carried out on desalination technology for water reuse. The conventional technologies which were applied for desalination include distillation [1,2], reverse osmosis (RO) [3,4], electrodialysis [5,6], ion exchange [7,8], and so on. Meanwhile, the ever-growing demand for energy saving and fresh water still requires a new desalination strategy with a lower cost, economic energy consumption, abundant material resources, a higher deionization capacity, and environmentally friendly features.

Capacitive deionization (CDI) is a desalination technique based on double layer capacitance theory. By applying a low DC voltage to two porous electrodes, an electrostatic field can be formed in the solution between the electrodes. The ions will move to the oppositely charged electrode under the action of an electric field to form an electrical double layer and are removed from the solution [9–13]. The electrodes' desorption regeneration can be achieved by simply shorting the circuit or reversing the polarity of the electrodes. CDI does not require an ion exchange membrane and a pressure difference, thus it is a promising

desalination technology which has multiple advantages over other desalinating processes: (i) this technique works by the process of electro-sorption and it is more energy-efficient as it does not require any high-pressure pumps; (ii) as the module works in a low applied voltage, it can be combined with solar/wind power and work in remote areas, where the availability of electricity is a major issue; (iii) the water reject is much less compared with other techniques such as RO; (iv) the carbon material can withstand a much higher temperature than the membranes, thereby it can be used for wider applications; and (v) as the device works like a capacitor, a high-energy recovery is possible [14,15].

The electrode material directly determines the ions adsorption capacity and adsorption rate, which is a key factor affecting the performance of the CDI. Carbon materials such as activated carbon and graphene are the most widely used electrode materials for CDI devices [16–18]. In recent years, carbon aerogel (CA), a lightweight nano-carbon material with a three-dimensional network, a large specific surface area, an abundant porosity, and a high electrical conductivity is expected to be another ideal electrode material. Xu et al. prepared CAs with resorcinol and formaldehyde and used them as CDI electrodes. The degree of ions adsorbed to the CA during the treatment of brackish water was found to be dependent upon the initial ion concentrations in the feed water with the following selectivity: I > Br > Ca > alkalinity > Mg > Na > Cl [19]. Li et al. provided a high-valence metal oxides-doped CA for the removal of toxic heavy metals from wastewater, exhibiting an outstanding decontamination capacity of 57.13 $mg \cdot g^{-1}$ for Cu(II) (50 $mg \cdot L^{-1}$ $CuCl_2$ solution) at a low applied voltage of 1.2 V [20]. Kumar et al. added tetraethylorthosilicate in the preparation of the CA and the obtained carbon-silicon composite aerogel through organo-inorganic co-assembly represented a good reusability in water desalination by CDI, observing that the ions desorbed completely after reversing the polarity [21].

Although a good desalination performance was achieved in the present application of CAs in the CDI, there are still some main drawbacks in the preparation of CAs. The commonly used precursors for CAs are toxic and the preparation process is complicated, which cannot meet the needs of large-scale production. Therefore, more facile and environmentally friendly strategy for the production of CAs is required. Furthermore, the porosity and specific surface area are important factors affecting the performance of the CDI electrode. An unavoidable agglomeration and structure collapse during the preparation of the CA would cause a partial loss of the surface activity. To improve the surface property of the material, an activation method based on alkali (KOH) is applied to tailor the microstructure of the CA and obtain activated carbon aerogels (ACAs) with ultrahigh specific surface areas and an adequate porosity in this study. At high temperature, KOH reacts with carbon atoms, leading to the reduction of hydroxyl anion into hydrogen gas and the oxidation of carbon into carbon monoxide. The consumption of carbons, the release of gases, and the production of potassium steam can widen the space between carbon layers and develop the network structure of CAs.

The purpose of this study is to prepare CAs from a non-toxic precursor with a simple and convenient method and activate CAs to offer a CDI electrode with a better desalination efficiency. In this study, the CAs were prepared using D(+)-glucose as a precursor, and the ACAs were obtained by a KOH activation. The morphology, surface area, porosity, surface groups, and composition of the CAs and ACAs were compared. Then, these electrodes were fabricated and characterized by a dynamic contact angle measurement and electrochemical properties analysis (cyclic voltammetry, electrochemical impedance spectroscopy). The NaCl removal performance by the two electrodes was compared, and the effects of the voltage, flow rate, and the NaCl concentration on the removal efficiency were studied. Finally, the regeneration property of the CDI electrode was investigated.

2. Experimental Section

2.1. Materials

D(+)-glucose was purchased from Sinoharm Chemical Reagent Co., Ltd., Shanghai, China. Hydrochloric acid was obtained from J&K Scientific Ltd., Beijing, China. Potas-

sium hydroxide was provided by Shanghai Aladdin Bio-Chem Technology Co., Ltd., Shanghai, China. Aniline was obtained from Sahn Chemical Technology Co., Shanghai, China. Sodium chloride was purchased from East China Normal University chemical plant, Tianjin, China.

2.2. Electrode Preparation

D(+)-glucose (10 g), potassium hydroxide (KOH, 1.225 g), and hydrochloric acid (HCl, 2.08 mL) were mixed into 25 mL of deionized water and were heated and stirred. When the temperature of the solution rose to 333 K, 0.5 mL of aniline was added to the mixture and then reacted at 433 K for 5 h. After cooling, aerogel was obtained by freeze-drying at 223 K for 72 h. Next, the aerogel was carbonized at a constant temperature of 1073 K for 2 h under nitrogen protection to obtain CA.

The CA was mixed with KOH at a mass ratio of 1:10 and soaked in 20 mL of deionized water for 12 h. After vacuum drying at 383 K for 24 h, the product was calcined at 1073 K for 1 h under nitrogen protection. After cooling, HCl was added and the mixture was washed with deionized water to achieve neutrality. The ACA was obtained after drying at 353 K for 24 h.

The electrode was prepared by adding CAs/ACAs, carbon black, and polytetrafluoroethylene (PTFE) to the mortar at a mass ratio of 8:1:1, and an appropriate amount of anhydrous ethanol was fully mixed and milled with the above materials. The product was rolled and cut to the desired size (about 4 $\times$ 4 cm) and then overlaid on a nickel foam plate for tableting, drying at 353 K for 24 h to obtain a CDI electrode. The weight of the active material (CA/ACA) was 0.1852 g and the thickness of the electrode material was 300 μm.

2.3. Design of CDI System and Measurement of NaCl Removal

The salt solution used in this experiment was a NaCl solution. The CDI system was operated in a cyclic desalination mode consisting of a CDI module, a DC stabilized power supply, a conductivity meter, a peristaltic pump, and a reservoir (Figure S1a). The specific experimental process was as follows: 35 mL of NaCl solution was withdrawn from the reservoir at a flow rate of 30 mL·min^{-1} and injected into the CDI module using a peristaltic pump. The solution flowed back to the reservoir after the treatment in the CDI module. In the CDI system, a conductivity meter probe was inserted in the reservoir to detect the total conductivity of the solution. When the adsorption on the electrodes reached equilibrium, a certain voltage was applied to the two electrodes of the CDI and the electro-sorption desalination started.

The basic structure of the CDI module is shown in Figure S1b. The components consisted of 1st polypropylene plate, 1st silicone rubber gasket, 1st CDI electrode, a silicone rubber gasket, 2nd CDI electrodes, 2nd silicone rubber gaskets, and 2nd polypropylene plates. The polypropylene plates were used to fix and support the CDI electrodes. The silicone rubber gaskets could seal and adjust the spacing and prevent the short circuit of the CDI electrodes. The CDI electrode is responsible for the removal of ions from the solution.

It is difficult to develop a real-time monitoring of the changes in the concentration of ions by a chemical measurement. When the temperature is kept constant, the concentration of the ions in the NaCl solution has a linear relationship with the conductivity in a certain concentration range. Therefore, the change in the ions' concentration in the solution can be analyzed through a real-time monitoring of the conductivity. In this study, 20, 50, 100, 200, 500, and 1000 mg·L^{-1} NaCl standard solutions were used to establish the relationship between the ions' concentration and conductivity. According to the linear fitting of the experimental data (Figure S2), the equation for the relationship between the concentration of the NaCl solution (y) and the conductivity (x) could be obtained as y = 0.5506x, with the correlation coefficient R^2 = 0.9997. These results showed that there was a good linear relationship between the concentration and conductivity of the NaCl solution in the range of 0~1000 mg·L^{-1}.

2.4. Characterization of Material

A morphological characterization of the CA and ACA was implemented using a ZEISS Merlin Compact field emission scanning electron microscope (SEM). To analyze the textural characteristics of the CAs and ACAs, low-temperature (77 K) nitrogen adsorption–desorption isotherms were recorded using a Micromeritics ASAP−2460 Surface Area and Porosity Analyzer. Fourier transformed infrared (FT-IR) spectroscopy (Nicoler Nexus 870, Thermo Scientific, Waltham, MA, USA) was employed to assess the functional groups and the structural changes. X-ray photoelectron spectroscopy (XPS) was conducted using the Thermo Scientific ESCALAB 250Xi to determine the composition of CA and ACA.

2.5. Characterization of Electrode

The hydrophilicity of the CAs and ACAs was tested by a JC2000DM contact angle meter. During the determination, 2 μL of water was dropped vertically on the electrode surface, the contact angle of the same electrode was tested 3 times, and the average value was calculated.

Cyclic voltammetry (CV) and electrochemical impedance spectroscopy (EIS) were performed with a CHI 670D electrochemical workstation to evaluate the electrochemical performance of the CA and ACA electrodes. A three-electrode system using the prepared CA/ACA electrode as the working electrode, the platinum wire as the counter electrode, the saturated calomel electrode as the reference electrode, and a 1 M NaCl solution as the electrolyte was adopted for the above analysis.

CV is a simple and convenient electrochemical technique that can be used to calculate the specific capacitance of an electrode material. In this experiment, the scan voltage range was −0.8 to 0 V and the scan rate was 5, 10, 20, and 50 $mV \cdot s^{-1}$, respectively. The specific capacitance value (C) of the electrode material was calculated according to Equation (1):

$$C = \frac{1}{2vm\left(V_f - V_i\right)} \int_{V_i}^{V_f} I(V)dV \quad (1)$$

where v is the scan rate ($mV \cdot s^{-1}$), m is the mass of electrode material (g), V_i and V_f are the starting and ending voltage (V) of the scan, respectively, and I is the current intensity (A).

EIS is often used to test the charge transfer resistance and ion diffusion behavior of the electrode. In this experiment, the frequency range was 0.01~10^5 Hz, the initial voltage was the open circuit voltage, and the amplitude was 5 mV.

2.6. CDI Experiments

The CA and ACA electrode were prepared in the same way and applied in the CDI system. To explore the effects of the electrode's spacing, voltage, flow rate, and salt concentration on desalination, different electrode spacings (2~6 mm) were constructed by adjusting the silicone rubber gaskets, different voltages (0.8 to 1.6 V) were applied to the CDI electrodes, different flow rates (10 to 50 $mL \cdot min^{-1}$) were regulated by a peristaltic pump, and different concentrations (100–500 $mg \cdot L^{-1}$) of the NaCl solutions were added to the CDI system. The solution concentration change was monitored by measuring the conductivity until the equilibrium was reached. The conditions of an electrode spacing of 2 mm, a flow rate of 30 $mL \cdot min^{-1}$, a DC voltage of 1.4 V, and a NaCl solution concentration of 100 $mg \cdot L^{-1}$ were selected to compare the desalination performance of CDI using CA and ACA.

To investigate the stability of the CDI electrode, 35 mL of NaCl solution with a concentration of 100 $mg \cdot L^{-1}$ was used in the CDI system, and a DC voltage of 1.4 V was applied. When the solution concentration dropped to a stable level, the electrodes were short circuited so that the ions adsorbed on the electrodes could return to the solution. When the solution concentration changed to the initial value, the electrodes regeneration was completed. The above operations were one process, the next process was performed after one process was completed, and these processes were repeated five times.

3. Results and Discussion

3.1. Characterization of CA and ACA

It can be seen from the SEM images (Figure S3) that the CAs and ACAs have a similar three-dimensional coral-like structure assembled by nanorods. After the KOH activation, the nanorods of the ACA (67 nm) became smaller in diameter than that of the CA (90 nm) and they were assembled more evenly. According to the N_2 adsorption–desorption isotherms and pore size distribution measurement (Figure S4), the CA and ACA showed a type I and II isotherm, respectively, and there were more mesopores and micropores in the ACAs. The specific surface area and total pore volume significantly increased from 567 $m^2 \cdot g^{-1}$ and 0.300 $cm^3 \cdot g^{-1}$ (CA) to 2413 $m^2 \cdot g^{-1}$ and 1.389 $cm^3 \cdot g^{-1}$ (ACA) after the activation treatment due to the etching effect of the KOH.

The CAs and ACAs had a similar FTIR spectra (Figure S5), but the relative intensity of the bands at 3422 cm^{-1} (stretching vibrations of O–H), 2921 cm^{-1} (stretching vibration of C–H), 1384 cm^{-1} (bending vibration of C–H), and 1126 cm^{-1} (bending vibration of C–O) increased after the activation, indicating that the ACA contained more oxygen-containing functional groups. XPS analysis (Figure S5) also demonstrated that the oxygen content increased from 6.35% to 12.14% due to the activation by the KOH. The C1s spectrum of the ACA showed a higher C–O (31.20%) and COOH (15.57%) content than that (23.01% and 7.49%) of the CA. The O1s spectra also indicated that the C–O–C and COOH content increased from 31.92% and 6.41% to 67.68% and 23.90%, respectively, after the activation. The increase in oxygen-containing functional groups would improve the hydrophilicity of the material.

3.2. Electrode Characterization

The contact angle meter was used to analyze the hydrophilicity of the CA and ACA electrodes. The water contact angle image is shown in Figure S6. The hydrophilicity of the material increased as the water contact angle decreased. When a contact angle is less than 90°, the material exhibits a hydrophilic character, while it is hydrophobic when the contact angle is larger than 90° [22]. From Figure S6, it can be observed that the contact angles of the CA and ACA were 118.54° and 69.31°, respectively, indicating that the CA was hydrophobic and the ACA was hydrophilic. It was clear that the hydrophilicity of the carbon aerogel significantly increased after the KOH activation. Perhaps alkali activation processes could introduce more oxygen-containing functional groups [23,24].

The electrochemical performance of the CDI electrode was closely related to its desalination effect. Generally, the electrode with a higher specific capacitance and a lower resistance tends to have a better desalination performance. In this study, the electrochemical performance of the CDI electrodes was tested using a three-electrode system. The CV characteristics of the CA and the ACA at 5, 10, 20, and 50 $mV \cdot s^{-1}$ are shown in Figure 1a,b. There was no regular rectangular shape in the CV diagram of the CA electrode, and a peak appeared at −0.35 V due to the Faradaic redox reaction, which showed that the capacitance behavior of the electrode was affected not only by the double layer effect but also by the pseudo capacitive effect [25,26]. The CV diagram of the ACA electrode exhibited a more obvious rectangular shape, indicating that the double layer effect dominated the capacitive behavior of the electrode. At the same time, it could also be observed that the specific capacitance of either the CA or the ACA electrode gradually decreased as the scan rate increased. When the scan rate increased from 5 $mV \cdot s^{-1}$ to 50 $mV \cdot s^{-1}$ and the specific capacitance of the CA and the ACA electrode decreased from 19.70 $F \cdot g^{-1}$ to 7.08 $F \cdot g^{-1}$ and 111.89 $F \cdot g^{-1}$ to 70.50 $F \cdot g^{-1}$, respectively, because the ions have more time to diffuse from the solution to the pores of the electrode at a low scan rate [27]. In addition, the specific capacity of the ACA electrode was almost six times that of the CA electrode at the same scan rate, indicating that the ACA electrode had a better electrochemical performance.

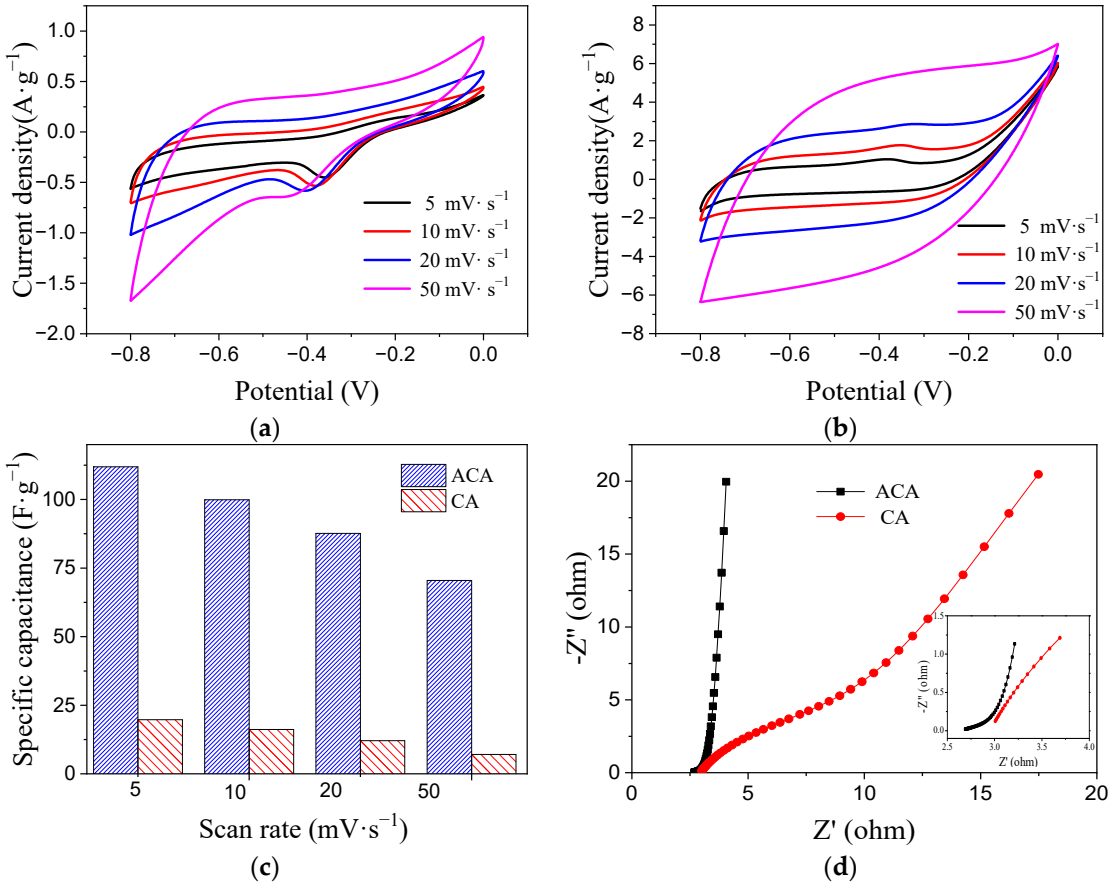

Figure 1. The CV curves of CA (**a**) and ACA (**b**) electrodes at different scan rates, their corresponding specific capacitance (**c**), and AC impedance Nyquist curves (**d**).

To investigate the difference in the conductivity of the CA and ACA electrode, an AC impedance test was performed, and the AC impedance Nyquist diagram is shown in Figure 1d. The Nyquist curve consists of a semi-arc in the high frequency region and a straight line in the low frequency region. The semi-arc in the high frequency region represents the charge transfer resistance at the interface between the solution and the electrode. The larger the semi-arc radius is, the greater the charge transfer resistance is [28]. The straight line in the low frequency region represents the ion diffusion behavior. The more vertical the line is, the better the double layer behavior is [29]. In the high frequency region, the semi-arc of the CA electrode had a larger radius, while the semi-arc of the ACA electrode was not obvious, indicating that the CA had a greater charge transfer resistance than the ACA electrode. At the same time, the intercept of the curve on the x-axis in the high-frequency region reflects the intrinsic resistance of the electrode, and the smaller the x-intercept is, the smaller the intrinsic resistance is [30]. It could be observed that the ACA electrode had a smaller intercept, showing its low intrinsic resistance. According to the above characterizations, the hydrophilicity of CA was improved significantly after the activation, which made the ACA electrode have a smaller charge transfer resistance. In addition, the ACA electrode with a more vertical straight line in the low frequency region had a better double layer behavior.

3.3. Desalination Performance of CDI Electrodes

The NaCl solution (100 mg·L^{-1}) was desalted using CDI based on the CA and ACA electrodes, respectively. As shown in Figure 2, the conductivity of the ACA system drops rapidly, and the electro-adsorption is already close to equilibrium at 15 min. While the conductivity of the CA system decreased slowly, it gradually approached equilibrium

at 20 min. The ACA electrode not only had a fast removal rate but also a greater total amount of the adsorption. The CA electrode could remove 17.7% of NaCl, and the salt adsorption capacity (SAC, q_t) and rate (SAR) was 3.66 $mg \cdot g^{-1}$ and 0.122 $mg \cdot g^{-1} \cdot min^{-1}$, respectively. The ACA electrode could remove 46.5% of NaCl, and the q_t and SAR was 9.73 $mg \cdot g^{-1}$ and 0.487 $mg \cdot g^{-1} \cdot min^{-1}$, which was about three and four times that of the CA electrode, respectively. It can be seen that the deionization performance of the CDI was greatly improved after the KOH activation modification of the CA, and the ACA electrode was more efficient and suitable for desalination.

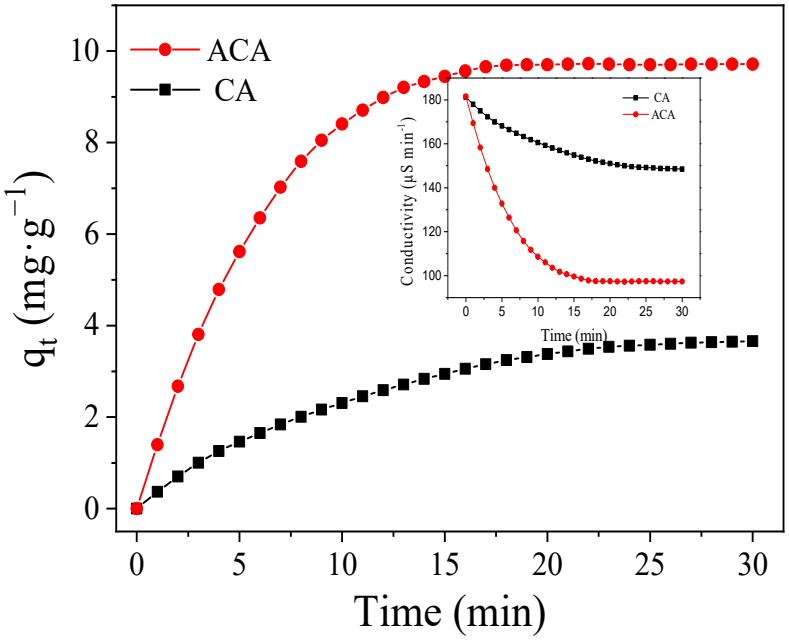

Figure 2. Desalination performance of CA and ACA electrodes.

At the same voltage, a different electrode spacing can produce a different electric field, which will affect the adsorption capacity of the CDI electrodes, so it is necessary to study the effect of electrode spacing on the desalination performance. In this study, CDI devices with electrode spacings of 2, 4, and 6 mm were used to analyze the desalination property of the ACA electrode. From Figure 3a, it can be observed that the desalination rate of the ACA electrode was 15.39, 22.27, and 41.34%, respectively, when the electrode spacing was 6, 4, and 2 mm. At the same applied voltage, the closer the electrodes are, the higher the desalination rate is, and the faster the solution conductivity decreases. The thickness of the diffuse electric double layer generated by the electrode increases, and the distance from the ions to the electric double layer becomes shorter as the electrode spacing is reduced, so the adsorption performance of the CDI is improved.

The voltage affects the electric field strength between the electrodes and the thickness of the electric double layer, thus affecting the desalination property of the electrode. In this study, different DC voltages (0.8–1.6 V) were applied to the CDI electrodes. As shown in Figure 3b, it was observed that the desalination rate of the ACA electrode increased from 11.72% to 30.14% as the applied voltage increased from 0.8 V to 1.4 V. When the voltage continued to increase to 1.6 V, the desalination rate of the electrode decreased to 22.06%. The higher the voltage is, the greater the electric field strength is, and the thicker the double layer is, the more pores of the electrode material which can be used by the ions in the solution increases, thus a higher number of ions are adsorbed. However, a high voltage will lead to a redox reaction of the solution at the electrode, which will reduce the utilization of the electrical energy, and then decrease the desalination efficiency and electro-sorption capacity [31]. In this study, 1.4 V was selected as the optimal voltage.

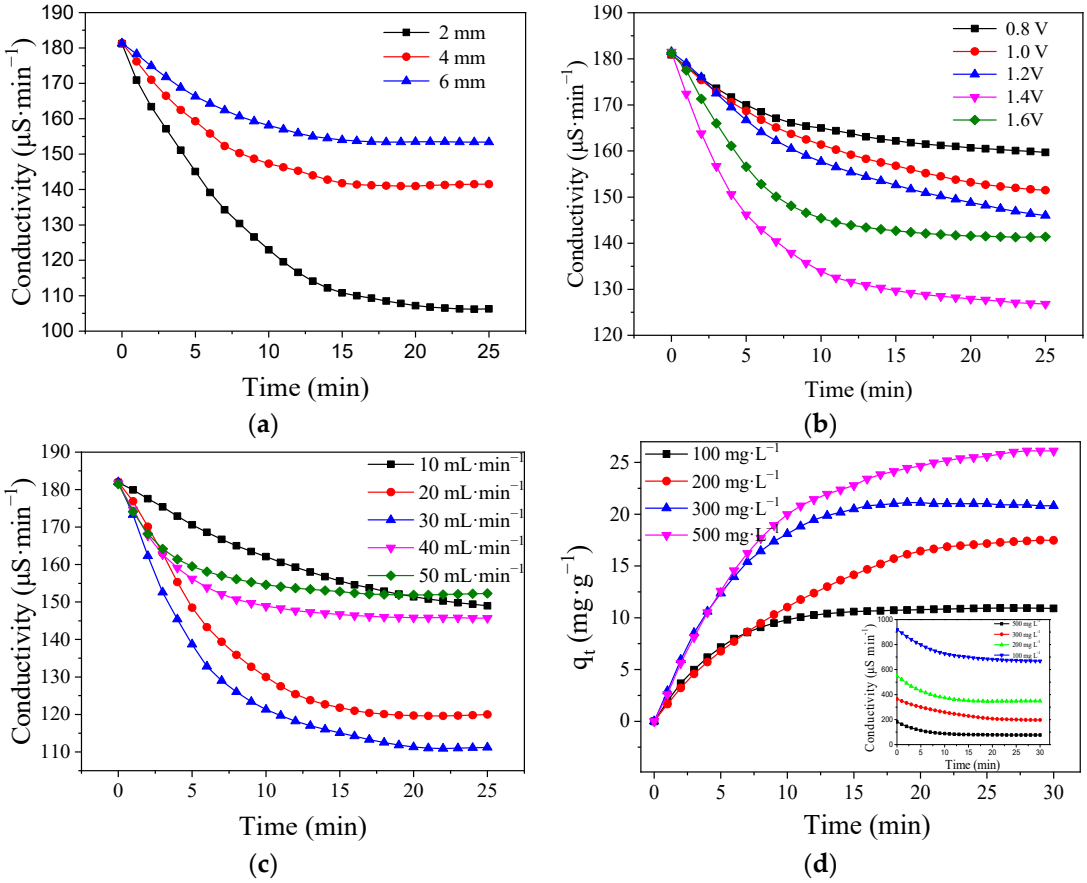

Figure 3. Effects of electrode spacing (**a**), applied voltage (**b**), volume flow rate (**c**), and NaCl concentration (**d**) on desalination performance.

It was found that the performance of the CDI was greatly affected by the volume flow rate of the solution. As shown in Figure 3c, the desalination rate of the ACA electrode increased from 18.09% to 39.07% firstly, and then decreased to 16.31% in the flow rate range of 10 to 50 mL·min^{-1}. This is due to the fact that the formation of the electric double layer is affected when the solution flows through the electrode. The double layer becomes thinner when the flow rate is too high. In addition, too high of a flow rate results in a shorter solution residence time and an insufficient contact between the ions in the solution and the electrode surface. These factors together lead to a decrease in the desalination rate. At a too low of a solution flow rate, the ions adsorbed on the surface of the electrode may be desorbed into solution due to the long residence time, also resulting in a lower desalination rate [32]. The optimal flow rate in this experiment was 30 mL·min^{-1}.

Electro-adsorption desalinations of 100, 200, 300, and 500 mg·L^{-1} NaCl solutions with the ACA electrode were also investigated, and the results are shown in Figure 3d. With the initial NaCl concentration increasing from 100 to 500 mg·L^{-1}, the desalination rate dropped from 57.90% to 27.31%, but the unit adsorption capacity of the ACA electrode increased from 10.95 mg·g^{-1} to 26.12 mg·g^{-1}, showing that the capacitance of the electric double layer was improved at a higher concentration of NaCl. When the initial concentration of NaCl was 500 mg·L^{-1}, the adsorption capacity of the CDI was 26.12 mg·g^{-1}, which was higher than those reported in many literatures (Table 1). For example, under the same experimental conditions, the adsorption capacity of the CDI using a functionalized graphene electrode in the study of Liu et al. was 13.72 mg·g^{-1} [33].

Table 1. Comparison of NaCl adsorption capability of ACA electrode and other electrode materials.

Electrode Materials	Adsorption Conditions	q_m ($mg \cdot g^{-1}$)	Reference
Carbon aerogel	1.2 V, 500 $mg \cdot L^{-1}$, 50 mL	15.7	[34]
Porous carbons	1.2 V, 500 $mg \cdot L^{-1}$, 30 mL	17.2	[35]
Activated carbon	1.5 V, 1000 $mg \cdot L^{-1}$, 50 mL	14.6	[36]
Porous carbon spheres	1.2 V, 500 $mg \cdot L^{-1}$, 20 mL	15.8	[37]
Graphene	1.4 V, 500 $mg \cdot L^{-1}$, 35 mL	13.7	[33]
Carbon sponge	1.2 V, 500 $mg \cdot L^{-1}$, 80 mL	16.1	[38]
Graphene	1.2 V, 100 $mg \cdot L^{-1}$	9.2	[39]
Carbon nanofiber	1.2 V, 1000 $mg \cdot L^{-1}$, 50 mL	12.8	[40]
Graphene	1.8 V, 100 $mg \cdot L^{-1}$, 50 mL	4.8	[41]
Porous carbon spheres	1.6 V, 500 $mg \cdot L^{-1}$, 50 mL	5.8	[42]
Graphitic porous carbon nanosheets	1.2 V, 500 $mg \cdot L^{-1}$	19.3	[43]
MoS_2−graphene	1.2 V, 500 $mg \cdot L^{-1}$, 50 mL	19.4	[18]
ACA	1.4 V, 500 $mg \cdot L^{-1}$, 35 mL	26.1	This study

The adsorption process and mechanism of the CDI based on the ACA electrode can be further understood by fitting the electro-adsorption data of different concentrations of the NaCl solution. The models of pseudo-first order and pseudo-second order were used to analyze the adsorption kinetics of the ACA electrode desalination. According to Table 2 (see SI Text S1 for the calculation method), it can be observed that the pseudo-first order model fits well with the kinetic data when the values of $q_{e,cal}$ and q_e are closer. The Langmuir and Freundlich isotherm models were used to fit the experimental data of the ACA electrode desalination. The fitting results are shown in Figure 4 and Table 3. The correlation coefficient (R^2) of the Langmuir model fitting was 0.99, which was higher than that of Freundlich, indicating that the Langmuir model could better fit the experimental data. The electro-adsorption of NaCl by the ACA electrode was a monolayer adsorption, and the theoretical adsorption capacity could reach 34.32 $mg \cdot g^{-1}$. The calculated separation factor (R_L) was 0.54 ($0 < R_L < 1$), indicating a favorable adsorption of NaCl (see SI Text S2 for calculation method) and the Langmuir isotherm was appropriate for this adsorption process [44].

Table 2. Kinetic parameters for ACA electrode desalination.

C_0 ($mg \cdot L^{-1}$)	q_e ($mg \cdot g^{-1}$)	Pseudo-First Order			Pseudo-Second Order			
		$q_{e,cal}$ ($mg \cdot g^{-1}$)	k_1 (min^{-1})	R^2	$q_{e,cal}$ ($mg \cdot g^{-1}$)	k_2 ($g \cdot mg^{-1} \cdot min^{-1}$)	h_0 ($mg \cdot g^{-1} \cdot min^{-1}$)	R^2
100	10.95	10.77	0.50	>0.99	13.09	0.0018	0.31	0.99
200	17.50	20.68	0.30	0.97	29.44	0.0006	0.56	>0.99
300	21.12	32.32	0.63	0.95	27.34	0.0003	0.22	0.98
500	26.12	27.27	0.33	>0.99	37.08	0.0002	0.27	0.98

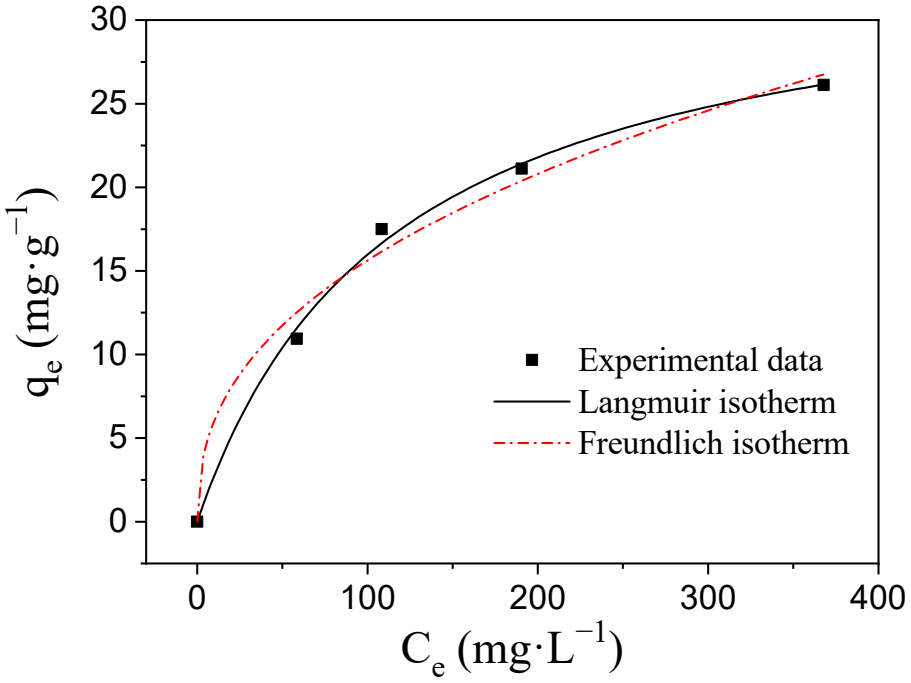

Figure 4. Adsorption isotherms of NaCl adsorbed by ACA.

Table 3. Parameters of Langmuir and Freundlich isotherm models for the adsorption of NaCl.

Models	Parameters	Values
Langmuir	q_m (mg·g^{-1})	34.32
	K_L (L·mg^{-1})	0.01
	R_L	0.54
	R^2	0.99
Freundlich	K_F ((mg·g^{-1}) (L·mg^{-1})$^{1/n}$)	2.34
	n	2.42
	R^2	0.98

3.4. Regeneration Property of ACA Electrode

An effective CDI requires not only a high adsorption capacity but also a good regeneration property. In this study, a 100 mg·L^{-1} NaCl solution was repeatedly desalted to test the reusability of the ACA electrode. When the NaCl concentration in the solution decreased to a stable level, the electrode was short-circuited and regenerated. The electro-adsorption procedure was repeated for stability testing. It can be seen from Figure 5 that the NaCl concentration could return to the initial value after short-circuiting the ACA electrode, showing a good regeneration property. In addition, there were still high desalination rates after the re-powering. After five adsorption and desorption cycles, the desalination rate of the CDI only decreased by 11%, indicating that the ACA electrode had a good reusability.

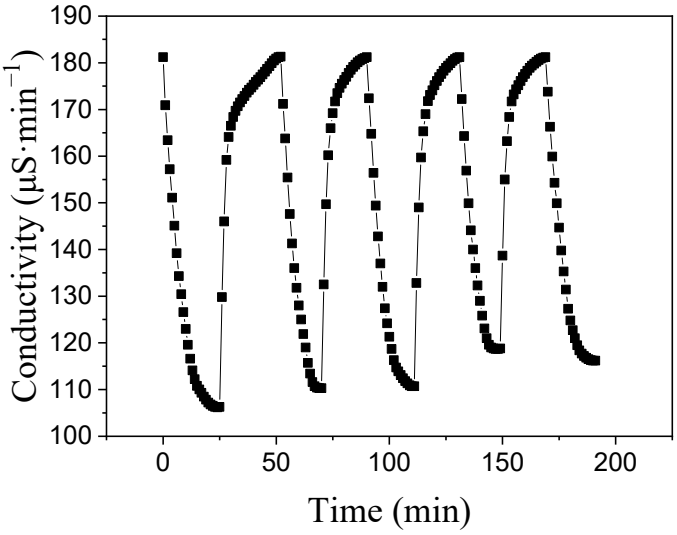

Figure 5. Regeneration properties of ACA electrodes.

4. Conclusions

Herein, CA was prepared by a facile and eco-friendly sol-gel approach from glucose, an abundant and inexpensive sugar molecule, and further activated by potassium hydroxide. The acquired ACA (contact angle: 69.31°) had a higher hydrophilicity than CA (contact angle: 118.54°). Correspondingly, the electrochemical performance of the CA was significantly improved after the activation. The ACA electrode had not only a higher specific capacitance (six times that of CA electrode) and better electric double layer behavior, but also a smaller charge transfer resistance and intrinsic resistance. Under the same experimental conditions, both the desalination rate and unit adsorption capacity of the ACA electrode was higher. In the desalination experiment of a 100 mg·L^{-1} NaCl solution, the adsorption capacity of the ACA electrode was three times of that of the CA electrode. In the CDI device based on the ACA electrode, the optimal electrode spacing for the desalination was 2 mm, the optimal voltage was 1.4 V, and the optimal flow rate was 30 mL·min^{-1}. When the NaCl concentration increased from 100 to 500 mg·L^{-1}, the unit adsorption capacity of the ACA electrode increased from 10.95 mg·g^{-1} to 26.12 mg·g^{-1}. The theoretical adsorption capacity determined by fitting to the Langmuir model was 34.32 mg·g^{-1}. A good regeneration of the ACA electrode could be achieved by short-circuiting the electrodes, and the ACA electrode remained a good cycle stability in five adsorption and desorption cycles.

Supplementary Materials: The following supporting information can be downloaded at: https://www.mdpi.com/article/10.3390/pr10112330/s1, Figure S1: Schematic diagram of (a) the CDI system and (b) the CDI module; Figure S2: Relationship between concentration and conductivity of NaCl solution; Figure S3: SEM images of CA (a) and ACA (b); Figure S4: N2 adsorption-desorption isotherms (a) and pore size distribution (b) of CA and ACA; Figure S5: FTIR (a) and XPS(b) spectra of CA and ACA, C 1s (c) and O 1s (d) high-resolution XPS spectra of CA, C 1s (e) and O 1s (f) high-resolution XPS spectra of ACA; Figure S6: Contact angles of CA (a) and ACA (b) electrodes.

Author Contributions: W.W.: conceptualization, data curation, writing—review and editing. K.L.: data curation, writing—original draft. G.S.: data curation. M.Z.: conceptualization, writing—review and editing. P.T.: data curation. All authors have read and agreed to the published version of the manuscript.

Funding: This research was funded by the Natural Science Foundation of Tianjin (No. 19JCYBJC23400 and 21JCZDJC00320), the National Natural Science Foundation of China (No. 21976096 and 22036004), the National Key Research and Development Program (No. 2018YFC1802000), and the NCC Fund.

Institutional Review Board Statement: Not applicable.

Informed Consent Statement: Not applicable.

Data Availability Statement: Not applicable.

Conflicts of Interest: The authors declare no conflict of interest or other interest that might be perceived to influence the results and/or discussion reported in this paper.

References

1. Dong, Y.X.; Poredoš, P.; Ma, Q.M.; Wang, R.Z. High-yielding and stable desalination via photothermal membrane distillation with free-flow evaporation channel. *Desalination* **2022**, *543*, 116103. [CrossRef]
2. Brogioli, D.; Yip, N.Y. Energy efficiency analysis of membrane distillation for thermally regenerative salinity gradient power technologies. *Desalination* **2022**, *531*, 115694. [CrossRef]
3. Fajardo-Diaz, J.L.; Morelos-Gomez, A.; Cruz-Silva, R.; Ishii, K.; Yasuike, T.; Kawakatsu, T.; Yamanaka, A.; Tejima, S.; Izu, K.; Saito, S.; et al. Low-pressure reverse osmosis membrane made of cellulose nanofiber and carbon nanotube polyamide nano-nanocomposite for high purity water production. *Chem. Eng. J.* **2022**, *448*, 137359. [CrossRef]
4. Biesheuvel, P.M.; Dykstra, J.E.; Porada, S.; Elimelech, M. New parametrization method for salt permeability of reverse osmosis desalination membranes. *J. Membr. Sci.* **2022**, *2*, 100010. [CrossRef]
5. Chen, Q.B.; Wang, J.Y.; Liu, Y.; Zhao, J.L.; Li, P.F. Novel energy-efficient electrodialysis system for continuous brackish water desalination: Innovative stack configurations and optimal inflow modes. *Water Res.* **2020**, *179*, 115847. [CrossRef]
6. Chen, Q.B.; Xu, Y.; Li, P.F.; Wang, J.; Dong, L.; Zhao, J.L.; Wang, J.Y. An emerging pilot-scale electrodialysis system for desalination of SWNF permeate: Evaluating the role of typical factors. *Desalination* **2022**, *542*, 116064. [CrossRef]
7. Wang, Z.D.; Tian, S.H.; Niu, J.J.; Kong, W.; Lin, J.Y.; Hao, X.G.; Guan, G.Q. An electrochemically switched ion exchange process with self-electrical-energy recuperation for desalination. *Sep. Purif. Technol.* **2020**, *239*, 116521. [CrossRef]
8. Subban, C.V.; Gadgil, A.J. Electrically regenerated ion-exchange technology for desalination of low-salinity water sources. *Desalination* **2019**, *465*, 38–43. [CrossRef]
9. Wu, Q.H.; Liang, D.W.; Lu, S.F.; Wang, H.N.; Xiang, Y.; Aurbach, D.; Avraham, E.; Cohen, I. Advances and perspectives in integrated membrane capacitive deionization for water desalination. *Desalination* **2022**, *542*, 116043. [CrossRef]
10. Toledo-Carrillo, E.; Zhang, X.Y.; Laxman, K.; Dutta, J. Asymmetric electrode capacitive deionization for energy efficient desalination. *Electrochim. Acta* **2020**, *358*, 136939. [CrossRef]
11. Zhang, C.Y.; He, D.; Ma, J.X.; Tang, W.W.; Waite, T.D. Faradaic reactions in capacitive deionization (CDI)-problems and possibilities: A review. *Water Res.* **2018**, *128*, 314–330. [CrossRef] [PubMed]
12. Pan, S.Y.; Haddad, A.Z.; Kumar, A.; Wang, S.W. Brackish water desalination using reverse osmosis and capacitive deionization at the water-energy nexus. *Water Res.* **2020**, *183*, 116064. [CrossRef] [PubMed]
13. Qin, M.; Deshmukh, A.; Epsztein, R.; Patel, S.K.; Owoseni, O.M.; Walker, W.S.; Elimelech, M. Comparing energy efficiency of capacitive deionization and reverse osmosis. *Desalination* **2019**, *455*, 100–114. [CrossRef]
14. Ahmed, M.A.; Tewari, S. Capacitive deionization: Processes, materials and state of the technology. *J. Electroanal. Chem.* **2018**, *813*, 178–192. [CrossRef]
15. Gupta, S.S.; Islam, M.R.; Pradeep, T. Capacitive Deionization (CDI): An alternative cost-efficient desalination technique. In *Advances in Water Purification Techniques, Meeting the Needs of Developed and Developing Countries*; Ahuja, S., Ed.; Elsevier/Ahuja Consulting: Calabash, NC, USA, 2019; Chapter 7, pp. 165–202.
16. Wu, L.; Liu, M.; Huo, S.; Zang, X.; Xua, M.; Ni, W.; Yang, Z.; Yan, Y.M. Mold-casting prepared free-standing activated carbon electrodes for capacitive deionization. *Carbon* **2019**, *149*, 627–636. [CrossRef]
17. Atoufi1, H.D.; Hasheminejad, H.; Lampert, D.J. Performance of activated carbon coated graphite bipolar electrodes on capacitive deionization method for salinity reduction. *Front. Environ. Sci. Eng.* **2020**, *14*, 99. [CrossRef]
18. Han, J.L.; Yan, T.T.; Shen, J.J.; Shi, L.Y.; Zhang, J.P.; Zhang, D.S. Capacitive deionization of saline water by using MoS_2–graphene hybrid electrodes with high volumetric adsorption capacity. *Environ. Sci. Technol.* **2019**, *53*, 12668–12676. [CrossRef]
19. Xu, P.; Drewes, J.E.; Heil, D.; Wang, G. Treatment of brackish produced water using carbon aerogel-based capacitive deionization technology. *Water Res.* **2008**, *42*, 2605–2617. [CrossRef]
20. Li, J.; Wang, X.; Wang, H.; Wang, S.; Hayat, T.; Alsaedi, A.; Wang, X. Functionalization of biomass carbonaceous aerogels and their application as electrode materials for electro-enhanced recovery of metal ions. *Environ. Sci. Nano* **2017**, *4*, 1114–1123. [CrossRef]
21. Kumar, R.; Sen Gupta, S.; Katiyar, S.; Raman, V.K.; Varigala, S.K.; Pradeep, T.; Sharma, A. Carbon aerogels through organo-inorganic co-assembly and their application in water desalination by capacitive deionization. *Carbon* **2016**, *99*, 375–383. [CrossRef]
22. Law, K.Y. Definitions for hydrophilicity, hydrophobicity, and superhydrophobicity: Getting the basics right. *J. Phys. Chem. Lett.* **2014**, *5*, 686–688. [CrossRef]
23. Wang, J.; Chen, S.; Xu, J.Y.; Liu, L.C.; Zhou, J.C.; Cai, J.J. High-surface-area porous carbons produced by the mild KOH activation of a chitosan hydrochar and their CO_2 capture. *Carbon* **2022**, *188*, 545. [CrossRef]
24. Acosta, R.; Fierro, V.; Martinez de Yuso, A.; Nabarlatz, D.; Celzard, A. Tetracycline adsorption onto activated carbons produced by KOH activation of tyre pyrolysis char. *Chemosphere* **2016**, *149*, 168–176. [CrossRef] [PubMed]
25. Forghani, M.; Donne, S.W. Method comparison for deconvoluting capacitive and pseudo-capacitive contributions to electrochemical capacitor electrode behavior. *J. Electrochem. Soc.* **2018**, *165*, A664. [CrossRef]

26. Lee, K.M.; Kim, K. Electrode potentials in electrochemical double-layer capacitors with asymmetric electrode thicknesses. *Electrochem. Electrochim. Acta* **2022**, *435*, 141364. [CrossRef]
27. Quan, X.; Fu, Z.; Yuan, L.; Zhong, M.; Mi, R.; Yang, X.; Yi, Y.; Wang, C. Capacitive deionization of NaCl solutions with ambient pressure dried carbon aerogel microsphere electrodes. *RSC Adv.* **2017**, *7*, 35875–35882. [CrossRef]
28. Kuo, H.A.; Ramachandran, A.; Oyarzun, D.I.; Clevenger, E.C.; Santiago, J.G.; Stadermann, M.; Campbell, P.G.; Hawks, S.A. Understanding resistances in capacitive deionization devices. *Environ. Sci. Water Res. Technol.* **2020**, *6*, 1842. [CrossRef]
29. Wang, H.; Yan, T.; Liu, P.; Chen, G.; Shi, L.; Zhang, J.; Zhong, Q.; Zhang, D. In situ creating interconnected pores across 3D graphene architectures and their application as high performance electrodes for flow-through deionization capacitors. *J. Mater. Chem. A* **2015**, *4*, 4908–4919. [CrossRef]
30. Zhao, S.; Yan, T.; Wang, H.; Zhang, J.; Shi, L.; Zhang, D. Creating 3D hierarchical carbon architectures with micro-, meso-, and macropores via a simple self-blowing strategy for a flow-through deionization capacitor. *ACS App. Mater. Interfaces* **2016**, *8*, 18027–18035. [CrossRef]
31. Maheshwari, K.; Agarwal, M.; Solanki, Y.S. Electrode material effect on electrochemical characterization, properties and operational parameters in capacitive deionization. *Mater. Today Proc.* **2021**, *43*, 1204–1209. [CrossRef]
32. Dahiya, S.; Mishra, B.K. Enhancing understandability and performance of flow electrode capacitive deionisation by optimizing configurational and operational parameters: A review on recent progress. *Sep. Purif. Technol.* **2020**, *240*, 116660. [CrossRef]
33. Liu, P.; Wang, H.; Yan, T.; Zhang, J.; Shi, L.; Zhang, D. Grafting sulfonic and amine functional groups on 3D graphene for improved capacitive deionization. *J. Mater. Chem. A* **2016**, *4*, 5303–5313. [CrossRef]
34. Luo, G.; Wang, Y.; Gao, L.; Zhang, D.; Lin, T. Graphene bonded carbon nanofiber aerogels with high capacitive deionization capability. *Electrochim. Acta* **2018**, *260*, 656–663. [CrossRef]
35. Li, Y.; Liu, Y.; Shen, J.; Qi, J.; Li, J.; Sun, X.; Shen, J.; Han, W.; Wang, L. Design of nitrogen-doped cluster-like porous carbons with hierarchical hollow nanoarchitecture and their enhanced performance in capacitive deionization. *Desalination* **2018**, *430*, 45–55. [CrossRef]
36. Xie, J.; Xue, Y.; He, M.; Luo, W.; Wang, H.; Wang, R.; Yan, Y.M. Organic-inorganic hybrid binder enhances capacitive deionization performance of activated-carbon electrode. *Carbon* **2017**, *123*, 574–582. [CrossRef]
37. Xu, X.; Tang, H.; Wang, M.; Liu, Y.; Li, Y.; Lu, T.; Pan, L. Carbon spheres with hierarchical micro/mesopores for water desalination by capacitive deionization. *J. Mater. Chem. A* **2016**, *4*, 16094–16100. [CrossRef]
38. Li, G.X.; Hou, P.X.; Zhao, S.Y.; Liu, C.; Cheng, H.M. A flexible cotton-derived carbon sponge for high-performance capacitive deionization. *Carbon* **2016**, *101*, 1–8. [CrossRef]
39. Wang, G.; Dong, Q.; Wu, T.; Zhan, F.; Zhou, M.; Qiu, J. Ultrasound-assisted preparation of electrospun carbon fiber/graphene electrodes for capacitive deionization: Importance and unique role of electrical conductivity. *Carbon* **2016**, *103*, 311–317. [CrossRef]
40. Liu, Y.; Lu, T.; Sun, Z.; Chu, D.C.; Pan, L. Ultra-thin carbon nanofiber networks derived from bacterial cellulose for capacitive deionization. *J. Mater. Chem. A* **2015**, *3*, 8693–8700. [CrossRef]
41. Xu, X.; Pan, L.; Liu, Y.; Lu, T.; Sun, Z. Enhanced capacitive deionization performance of graphene by nitrogen doping. *J. Colloid Interface Sci.* **2015**, *445*, 143–150. [CrossRef]
42. Liu, Y.; Pan, L.; Chen, T.; Xu, X.; Lu, T.; Sun, Z.; Chua, D.H.C. Porous carbon spheres via microwave-assisted synthesis for capacitive deionization. *Electrochim. Acta* **2015**, *151*, 489–496. [CrossRef]
43. Wang, H.; Yan, T.; Shen, J.; Zhang, J.; Shi, L.; Zhang, D. Efficient removal of metal ions by capacitive deionization with straw waste derived graphitic porous carbon nanosheets. *Environ. Sci. Nano* **2020**, *7*, 317–326. [CrossRef]
44. Li, C.P.; Wu, Y.Q.; Zhang, F.Y.; Gao, L.X.; Zhang, D.Q.; An, Z.X. Capacitive deionization of NaCl solution with hierarchical porous carbon materials derived from Mg-MOFs. *Sep. Purif. Technol.* **2021**, *277*, 119618. [CrossRef]